

Theoretical Study of Reactivity Indices and Rough Potential Energy Curves for the Dissociation of 59 Fullerendiols in Gas-Phase and in Aqueous Solution with an Implicit Solvent Model

Anne Justine ETINDELE *Higher Teachers Training College, University of Yaounde I, P.O. Box 47, Yaounde, CAMEROON*
e-mail: annetindele@yahoo.fr

Abraham PONRA
Department of Physics, Faculty of Science, University of Maroua, P.O. Box 814, Maroua, CAMEROON
e-mail: abraPONRA@yahoo.com

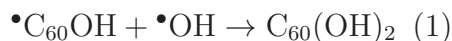
Mark E. CASIDA
Laboratoire de Spectrométrie, Interactions et Chimie théorique (SITh), Département de Chimie Moléculaire (DCM, UMR CNRS/UGA 5250), Institut de Chimie Moléculaire de Grenoble (ICMG, IR2607), Université Grenoble Alpes (UGA) 301 rue de la Chimie, BP 53, F-38041 Grenoble Cedex FRANCE
e-mail: mark.casida@univ-grenoble-alpes.fr

Dr. Andrés CISNEROS
Department of Physics, Department of Chemistry and Biochemistry, University of Texas at Dallas, Richardson, Texas, 75802, USA
e-mail: andres@utdallas.edu

Jorge NOCHEBUENA
Department of Chemistry and Biochemistry, College of Science and Mathematics, Augusta University, Augusta, Georgia, 30912, USA
e-mail: jnochebuenaherna@augusta.edu

Abstract

Buckminsterfullerene, C_{60} , has not only a beautiful truncated icosahedral (soccerball) shape, but simple Hückel calculations predict a three-fold degenerate lowest unoccupied molecular orbital (LUMO) which can accommodate up to six electrons making it a good electron acceptor. Experiments have confirmed that C_{60} is a radical sponge and it is now sold for use in topical cosmetics. Further medical uses require functionalization of C_{60} to make it soluble and one of the simplest functionalizations is to make $C_{60}(OH)_n$ fullerenols. A previous article [*Adv. Quant. Chem.* **8**, 351 (2023)] studied reactivity indices for the successive addition of the $\bullet OH$ radical to $(\bullet)C_{60}(OH)_n$ in gas phase. [$(\bullet)C_{60}(OH)_n$ is only a radical when n is an odd number.] This present article extends this previous work by examining various aspects of how the reaction,



changes in aqueous solution. One obvious difference between C_{60} and their various isomers of $C_{60}(OH)_2$ is the presence of a dipole. As fullerendiols are nearly spherical, their change in dipole moment in going from gas to aqueous phase may be estimated using back-of-the-envelope calculations

with the Onsager model. The result is remarkably similar to what is obtained using density-functional theory (DFT) with an implicit solvation model (Surface Molecular Density, SMD). Calculation of fullerendiol C-O bond energies and reactivity indices using the SMD approach confirm that the general conclusions from the earlier work regarding gas-phase reactivity still hold in the aqueous phase. A major difference between the present work and the earlier work is the calculation of potential energy curves (PECs) for reaction (1) in gas and aqueous phases. This is done in exploratory work for all 59 possible fullerendiols in both gas phase and in aqueous solution with the SMD approach using spin-unrestricted DFT calculations with symmetry breaking. Surprisingly little change is found between the gas-phase and aqueous-phase PECs. It is discovered that the majority of $C_{60}(OH)_2$ show radicaloid character, as might have been expected from trying to draw resonance structures. Spin-contamination curves are also remarkably similar for gas-phase and aqueous-phase results. Although our calculations do not include a dispersion correction, it was noticed that all calculated PECs have a $1/R^6$ behavior over a significant $R = R(C-O)$ distance, underlying the need to be careful of double counting when including dispersion corrections in DFT. A short coming of our SMD approach is the lack of explicit water molecules which can form hydrogen bonds with the OH groups and dissociating radicals.

1 Introduction

Buckminsterfullerene C_{60} is well-known for its geometrical beauty, reminiscent of the geodesic domes of Buckminsterfuller. It can also capture up to six electrons in its t_{1u} lowest unoccupied molecular orbitals (LUMOs). This strongly electrophilic property has been characterized experimentally and it has been called a “radical sponge” [1]. It is even used as a commercial ingredient in some skin care products, one of which is an anti-aging moisturizer which goes by the name “C60” [2]. However many applications require an increase in the aqueous solubility of this hydrophobic molecule. A particularly simple way to increase the solubility of C_{60} is to decorate it with hydroxyl groups. As C_{60} is a “radical sponge,” it can react with a large number of hydroxyl radicals [3, 4, 5, 6, 7, 8, 9, 10, 11, 12, 13, 14, 15, 16] to create fullereneols ($\bullet C_{60}(OH)_n$) where the bullet (\bullet) is a reminder that these fullereneols are radicals for odd n .

C_{60}

LUMO

To take into account the impact of solvents on the properties of molecules, two approaches may be considered. The first approach takes the molecular nature of the solvent molecules explicitly into account. We will only use the second in the present work. This is the implicit model in which the solvent is considered as a dielectric continuum. As the $\bullet C_{60}(OH)_n$ are nearly spherical, Onsager’s spherical dielectric cavity reaction field model provides a pencil and paper way to determine the dipole moment for the molecule in solution from its gas-phase dipole moment. Thus Onsager’s spherical dielectric cavity reaction field model provides a pencil and paper way to determine the dipole moment for the molecule in solution from its gas-phase dipole moment. This first-order approximation works almost surprisingly well compared to other implicit solvent models that use cavities which are more carefully adjusted to reflect the shape of the molecule.

The global and local reactivity indices can be significantly impacted depending on whether the study is carried out in the gas or aqueous phase [17, 18]. These reactivity indices made it possible to effectively study the donor and acceptor character of $C_{60}(OH)_n$ [16] in the gas phase. So, what about this character for the aqueous phase? We are given the opportunity to try to answer this question in this paper. In addition, the description of potential energy curves (PECs) could provide valuable information on the impact of the presence of the solvent on the dissociation (or formation) of the fullereneol-hydroxyl (i.e., $\bullet C_{60}(OH) + \bullet OH$) bonds.

PEC

Previous work has shown that the dissociation of a molecule into two fragments requires taking into account symmetry breaking along the PECs [19, 20]. Taking into account this symmetry breaking, point-by-point, throughout the PECs provides a unique opportunity to determine the Coulson-Fisher points for the 59 isomers of fullerenediol by examining the variation of $\langle \hat{S}^2 \rangle$ with distance.

This article is organized in the following manner: The next section covers the basic theory used in the rest of the paper. Section 3 gives the computational details that we are using in this paper for all the calculations. Section 4 presents and discusses our results. In particular, we present PECs and their associated $\langle \hat{S}^2 \rangle$ for all 59 isomers in the SI. Section 5 is the concluding discussion.

2 Theory

Electronic structure calculations were initially done for atoms, gradually moved onto small molecules, and then—with the development of band theory—onto crystals. However it is important to be able to model the electronic structure of solvated molecules for the simple reason that most experiments are carried out in solution, or at least involve key steps and/or measurements carried out in solution. We use an implicit solvent model. This replaces the solvent with a dielectric cavity. It has the advantage

of being relatively simple and so computationally expedient, but does not take into account all of the physics of a molecule in solution.

The implicit solvent model used in the present work is the well-known SMD (for Solvation Model based upon the quantum mechanical Density) [21]. This is a reaction field model where the solvent molecules are replaced by a dielectric continuum surrounding the solvated molecules in a solvent excluded cavity (SEC, also said to be defined by a solvent accessible surface). The molecule in the cavity is described by quantum mechanics (QM), from which its charge distribution is calculated. This charge distribution creates a reaction field in the surrounding dielectric which, in turn, modifies the QM calculation. Although this sounds like it requires an iterative self-consistent calculation, its solution may be done in a non-iterative single-step procedure. Particular implicit solvent models vary by how the SEC is generated and how the Poisson equation is solved to determine the reaction field. In particular, the generation of the SEC involves some semi-empirical parameters which are fit, in the SMD model, to experimental solvation free energies. It is not our purpose to go further into details here.

SMD

SEC

QM

However fullerenediols are nearly spherical molecules which means that the oldest most approximate reaction field model—namely the Onsager model [22] is expected to be a good approximation. Although a program such as GAUSSIAN [23] has an option to do Onsager reaction field calculations, it is really a shame to use such a large program for what is ultimately a back-of-the-envelope calculation. Indeed, doing the back-of-the-envelope calculation leads to enhanced understanding and so we do present this model here. As with more sophisticated implicit solvent models, the solvent is treated as a polarizable continuum with dielectric constant ϵ . However the molecule is treated as a point dipole moment μ_ℓ whose value will depend upon its surroundings. It also has a polarizability α . The molecule is placed in a solvent-excluded spherical cavity of radius a . The electric field of the molecular dipole moment will cause a redistribution of charges around the sphere and induce a reaction (electric field) $\vec{\mathcal{E}}$ inside the sphere which acts on the molecule to change the dipole moment through the equation,

$$\vec{\mu}_\ell = \vec{\mu}_g + \alpha \vec{\mathcal{E}}, \quad (1)$$

where $\vec{\mu}_\ell$ is the molecular dipole moment in the liquid and μ_g is the gas-phase dipole moment. This reaction field is (Ref. [24] pp. 130-134)

$$\vec{\mathcal{E}} = \frac{2(\epsilon - 1)}{2\epsilon + 1} \frac{1}{a^3} \vec{\mu}_\ell. \quad (2)$$

Therefore,

$$\vec{\mathcal{E}} = \frac{2(\epsilon - 1)}{2\epsilon + 1} \frac{1}{a^3} (\vec{\mu}_g + \alpha \vec{\mathcal{E}}), \quad (3)$$

which can be solved for the reaction field to give,

$$\vec{\mathcal{E}} = \left(\frac{2\epsilon + 1}{2(\epsilon - 1)} a^2 \mathbf{1} - \alpha \right)^{-1} \vec{\mu}_g. \quad (4)$$

Finally, plugging this result into Eq. (1) and rearranging gives,

$$\vec{\mu}_\ell = \left(\mathbf{1} - \frac{2(\epsilon - 1)}{2\epsilon + 1} \frac{1}{a^3} \alpha \right)^{-1} \vec{\mu}_g. \quad (5)$$

This still leaves the problem of the polarizability and the size of the cavity. However assuming an isotropic medium, so that we may replace the polarizability tensor α with the average polarizability

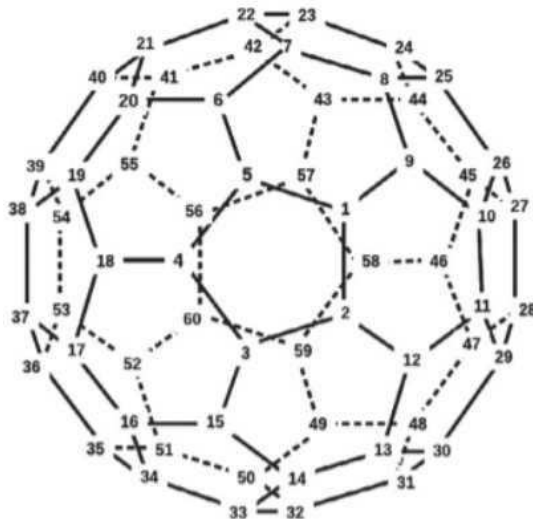


Figure 1: IUPAC numbering of buckminsterfullerene [27].

$\bar{\alpha}$, gives,

$$\vec{\mu}_\ell = \left(1 - \frac{2(\epsilon - 1)}{2\epsilon + 1} \frac{\bar{\alpha}}{a^3}\right)^{-1} \vec{\mu}_g, \quad (6)$$

so that we actually only need to determine $\bar{\alpha}/a^3$. This can be done using the Lorenz-Lorentz equation relating the polarizability and the refractive index n ,

$$\frac{n^2 - 1}{n^2 + 2} = \frac{4\pi}{3} \rho \bar{\alpha}, \quad (7)$$

where ρ is the number density so that,

$$\frac{1}{\rho} = \frac{4}{3} \pi a^3. \quad (8)$$

Hence,

$$\frac{\bar{\alpha}}{a^3} = \frac{n^2 - 1}{n^2 + 2}. \quad (9)$$

Note that using these equations for treating C_{60} in water requires the dielectric constant for water but the refractive index of C_{60} . For water, $\epsilon = 80$ at 20 °C (Ref. [25], p. 299). The refractive index of solid C_{60} which is 2.2 at 630 nm wavelength [26]. Putting everything together, then

$$\vec{\mu}_\ell = 2.23 \vec{\mu}_g. \quad (10)$$

for C_{60} in aqueous solution. We expect similar results for fullerenols.

3 Computational Details

The International Union of Pure and Applied Chemistry (IUPAC) numbering (**Fig. 1**) is used throughout for C_{60} [27]. An “xyz” format file with this numbering has been supplied in the Electronic Supplementary Information (ESI) for use with molecular visualization software.

IUPAC
ESI

The same level of electronic structure calculation is used throughout this article, whether it be for the gas-phase or for the aqueous phase using an implicit solvent model.

Calculations were carried out using version 5.0.4 of ORCA [28] and with GAUSSIAN [23]. The B3LYP keyword was used with GAUSSIAN while the B3LYP/g keyword was used with ORCA. This is the same functional which we will rename B3LYP(VWN3) [29, 30] because the original B3LYP functional (programmed in GAUSSIAN) used the Vosko-Wilk-Nusair parameterization of the random-phase approximation correlation energy (known as VWN3 in GAUSSIAN) but that the default B3LYP functional in ORCA uses the Vosko-Wilk-Nusair parameterization of the Ceperley and Alder’s quantum Monte Carlo correlation energy (known as VWN5 in GAUSSIAN) unless “/g” is specified. The same def2SVP [31] orbital basis set was used in all our calculations.

The default in ORCA is also to use a resolution-of-the-identity (RI) approximation to reduce the problem of calculating four-center electron repulsion integrals to that of calculating only three-center electron repulsion integrals. As this option was used in our previous gas-phase work [16] on gas-phase reactivity indices, we continued with the same option in the article when calculating reactivity indices in solution. It was also used in calculating gas and solution phase dipole moments. However it was judged useful to follow the advice of Ref. [32] in order to ensure the best possible agreement between ORCA and GAUSSIAN calculations:

RI

“ In ORCA, keywords used included `NORI` (no approximation is used), `TightSCF`, `TightOpt`, `SlowConv`, `NumFreq` and an ultra-fine grid. We explicitly confirmed that GAUSSIAN and ORCA gave the same results for the same basis sets and functionals in single-point calculations.” [32]

Implicit solvent calculations were carried out with ORCA [28] at the B3LYP(VWN3)/def2-SVP level using the SMD [21] solvent model. It has been discovered, in work on polypyridine ruthenium clusters, that GAUSSIAN and ORCA use different grids on the solvent-allowed surface which leads to significant differences in numerical results (see the ESI of Ref. [33]). Following that work, we opted to use

```
%cpcm
num_leb 590
end
```

in the ORCA input to in order ensure good agreement with GAUSSIAN.

4 Results

A thorough study of the gas-phase reactivity of fullerenols with respect to step-wise addition of hydroxyl radicals has already been presented in Ref. [16]. Our interest here is in how the physical and chemical properties of fullerenols differ in gas phase and in aqueous solution. We will confine our study to fullerenediols only. As **Table 1** shows, this is still a very large number of isomers. We will begin with physical properties and then chemical reactivity indices before going on to potential energy curves (PECs) for the dissociation reaction,

PEC



Count	Symmetry-Equivalent Isomers	Distance
2	(1,2)-C ₆₀ (OH) ₂ , (1,5)-C ₆₀ (OH) ₂	1 bond
+2 = 4	(1,3)-C ₆₀ (OH) ₂ , (1,4)-C ₆₀ (OH) ₂	2 bonds
+2 = 6	(1,6)-C ₆₀ (OH) ₂ , (1,12)-C ₆₀ (OH) ₂	2 bonds
+2 = 8	(1,7)*-C ₆₀ (OH) ₂ , (1,11)*-C ₆₀ (OH) ₂	3 bonds
+2 = 10	(1,8)*-C ₆₀ (OH) ₂ , (1,10)*-C ₆₀ (OH) ₂	2 bonds
+1 = 11	(1,9)-C ₆₀ (OH) ₂	1 bond
+2 = 13	(1,13)-C ₆₀ (OH) ₂ , (1,20)-C ₆₀ (OH) ₂	3 bonds
+2 = 15	(1,14)-C ₆₀ (OH) ₂ , (1,19)-C ₆₀ (OH) ₂	4 bonds
+2 = 17	(1,15)*-C ₆₀ (OH) ₂ , (1,18)*-C ₆₀ (OH) ₂	3 bonds
+2 = 19	(1,16)-C ₆₀ (OH) ₂ , (1,17)-C ₆₀ (OH) ₂	4 bonds
+2 = 21	(1,21)-C ₆₀ (OH) ₂ , (1,30)-C ₆₀ (OH) ₂	4 bonds
+2 = 23	(1,22)*-C ₆₀ (OH) ₂ , (1,29)*-C ₆₀ (OH) ₂	4 bonds
+2 = 25	(1,23)-C ₆₀ (OH) ₂ , (1,28)-C ₆₀ (OH) ₂	5 bonds
+2 = 27	(1,24)*-C ₆₀ (OH) ₂ , (1,27)*-C ₆₀ (OH) ₂	4 bonds
+2 = 29	(1,25)-C ₆₀ (OH) ₂ , (1,26)-C ₆₀ (OH) ₂	3 bonds
+2 = 31	(1,31)-C ₆₀ (OH) ₂ , (1,40)-C ₆₀ (OH) ₂	5 bonds
+2 = 33	(1,32)*-C ₆₀ (OH) ₂ , (1,39)*-C ₆₀ (OH) ₂	6 bonds
+2 = 35	(1,33)*-C ₆₀ (OH) ₂ , (1,38)*-C ₆₀ (OH) ₂	5 bonds
+2 = 37	(1,34)*-C ₆₀ (OH) ₂ , (1,37)*-C ₆₀ (OH) ₂	5 bonds
+2 = 39	(1,35)-C ₆₀ (OH) ₂ , (1,36)-C ₆₀ (OH) ₂	6 bonds
+2 = 41	(1,41)-C ₆₀ (OH) ₂ , (1,48)-C ₆₀ (OH) ₂	6 bonds
+2 = 43	(1,42)-C ₆₀ (OH) ₂ , (1,47)-C ₆₀ (OH) ₂	6 bonds
+2 = 45	(1,43)-C ₆₀ (OH) ₂ , (1,46)-C ₆₀ (OH) ₂	6 bonds
+2 = 47	(1,44)-C ₆₀ (OH) ₂ , (1,45)-C ₆₀ (OH) ₂	5 bonds
+2 = 49	(1,49)-C ₆₀ (OH) ₂ , (1,55)-C ₆₀ (OH) ₂	7 bonds
+2 = 51	(1,50)-C ₆₀ (OH) ₂ , (1,54)-C ₆₀ (OH) ₂	7 bonds
+2 = 53	(1,51)-C ₆₀ (OH) ₂ , (1,53)-C ₆₀ (OH) ₂	6 bonds
+1 = 54	(1,52)-C ₆₀ (OH) ₂	8 bonds
+2 = 56	(1,56)*-C ₆₀ (OH) ₂ , (1,59)*-C ₆₀ (OH) ₂	8 bonds
+2 = 58	(1,57)-C ₆₀ (OH) ₂ , (1,58)-C ₆₀ (OH) ₂	7 bonds
+1 = 59	(1,60)-C ₆₀ (OH) ₂	9 bonds

Table 1: List of symmetry equivalent (mirror image) isomers. The distance is the shortest through-bond distance. Isomers with an asterisk (*) are symmetry pairs with significant disagreement in their energy at $R(\text{C-O}) = 1.4 \text{ \AA}$ (see text).

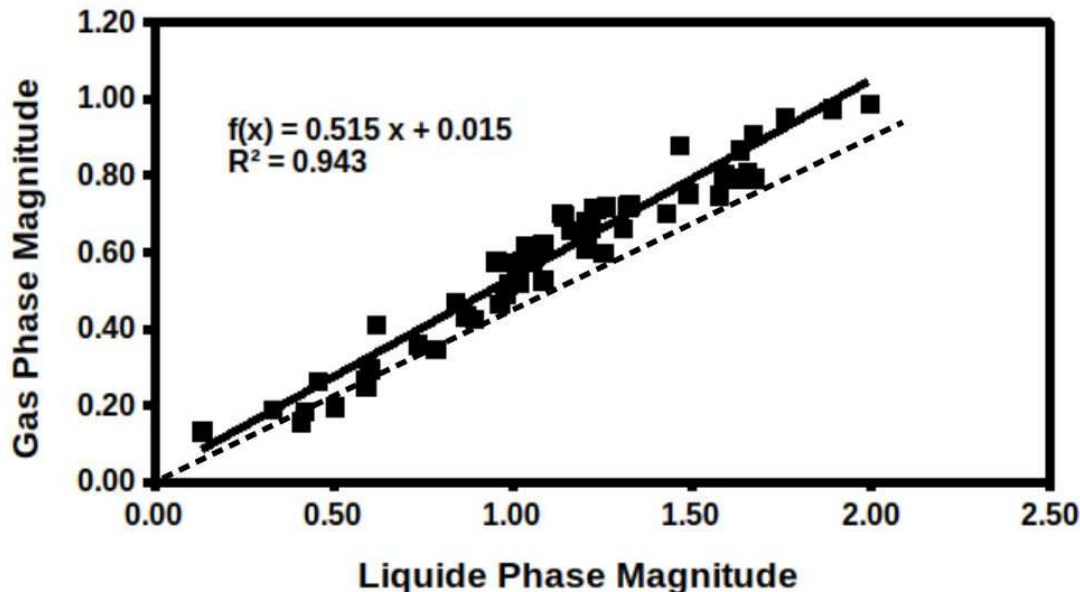


Figure 2: Graph correlating the magnitudes of gas-phase and SMD aqueous-phase dipole moments for $C_{60}(OH)_2$ fullerenols calculated using geometries optimized in the gas phase. The dashed line is the result of Onsager’s implicit solvent model. See text.

Dipole moments SMD implicit solvent calculations of the dipole moments of the fullerenediols in solution were carried out at the spin-restricted (same-orbitals-for-different-spins or SODS) level using geometries optimized in the gas phase. The simplest implicit solvent model is the Onsager model which we expect to be a good first approximation for fullerenediols. This is confirmed in **Fig. 2** where we present a correlation plot between calculated gas-phase and aqueous-phase dipole moments. The Onsager model predicts a straight line passing through the origin and with slope,

SODS

$$m = 1 - \left(\frac{2(\epsilon - 1)}{2\epsilon + 1} \right) \left(\frac{n^2 - 1}{n^2 + 2} \right). \quad (12)$$

Here ϵ is the dielectric constant of the surrounding water, which is well-known to be close to 80, and n is the refractive index of solid C_{60} which is 2.2 at 630 nm wavelength [26]. Using these values gives a slope of $m = 0.44906$ which corresponds to the dashed line in Fig. 2. We can conclude that the Onsager model is a reasonable first approximation to the SMD implicit solvent model in this case.

Reactivity indices Given such a large change in the dipole moments going between the gas- and aqueous-phases, we might also expect a large change in reactivity indices. As in Ref. [16], we seek how well reactivity indices predict the C-O bond dissociation energy (BDE). This latter is calculated as the difference between the sum of the spin-unrestricted (different-orbital-for-different-spins or DODS) energies of $\bullet C_{60}(OH) + \bullet OH$ and the SODS energy of $C_{60}(OH)_2$. The gas-phase results confirmed that the BDE energy increases (i.e., the fullerenediol becomes more stable) as the spin density of the reaction site $\bullet C_{60}(OH)$ increases. Part (a) of **Fig. 3** shows that this also holds in our solution study. The gas-phase results also confirmed the electrophilic nature of the $\bullet OH$ radical because larger BDEs were generally found at sites with more negative Mulliken charges. Part (b) of Fig. 3 shows that this continues to hold in aqueous solution. Finally large values of the radical Fukui function f^0 were also found to favor large values of the BDE in the gas phase and part (c) of Fig. 3 shows that this

BDE
DODS

continues to hold in aqueous solution. That the SMD aqueous solution results look very much like the corresponding gas-phase results [16] is a nice confirmation that $\bullet\text{OH}$ remains an electrophilic radical in solution even with respect to an “electron sponge” such as C_{60} .

Exploratory study of PECs The large number of fullerenediol isomers (not to mention their various conformers!) shown in Table 1 represents a serious complication for studying the PECs for reaction 11. In order to keep things manageable, we have chosen to only calculate PECs for rigid vertical removal of $\bullet\text{OH}$ without any internal relaxation of either $\bullet\text{C}_{60}\text{OH}$ or $\bullet\text{OH}$ (**Fig. 4**).

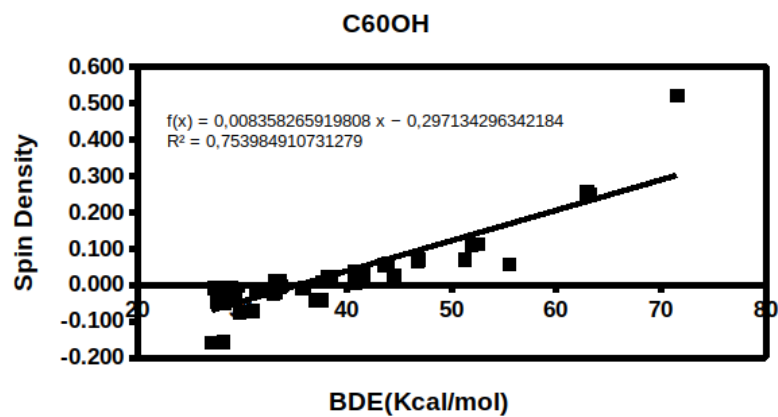
Calculations were of the spin-unrestricted (DODS) type with symmetry breaking so as to be able to describe the breaking of the C-O single bond as correctly as possible. Both energies and spin contamination ($\langle\hat{S}^2\rangle$) were monitored. This produced much too many results to given in the main body of the paper so we will just give a few examples and some summarizing statistics. Full results may be found in the Supplementary Information (SI) associated with this article. What we expected to see were curves such as those found for 1,5- $\text{C}_{60}(\text{OH})_2$ and shown in **Fig. 5**. At large $R(\text{C-O})$, we expect to see a heavily spin-contaminated open-shell singlet with $\langle\hat{S}^2\rangle \approx 1$. As the $\bullet\text{C}_{60}(\text{OH})$ and $\bullet\text{OH}$ radicals approach and form a bond, we expected a normal closed-shell singlet with $\langle\hat{S}^2\rangle = 0$. Interestingly, this only happened for about a quarter of the symmetry pairs studied.

Much like with the reactivity indices, the PECs and spin-contamination curves turn out to be remarkably similar in gas-phase and in aqueous solution. The degree of spin contamination for the different isomers is shown in **Fig. 7**. It is apparent that there are many fullerediols which are not simple closed-shell singlets. At first thought, this may be a bit surprising as such structures are rarely mentioned in the relevant literature. On second thought, it is easy to understand why radicaloid structures might be preferred in many cases. One such structure is illustrated in **Fig. 6** and has been verified by examination of the spin density of 1,8- $\text{C}_{60}(\text{OH})_2$. In contrast, both 1,7- $\text{C}_{60}(\text{OH})_2$ and 1,9- $\text{C}_{60}(\text{OH})_2$ are closed-shell singlets.

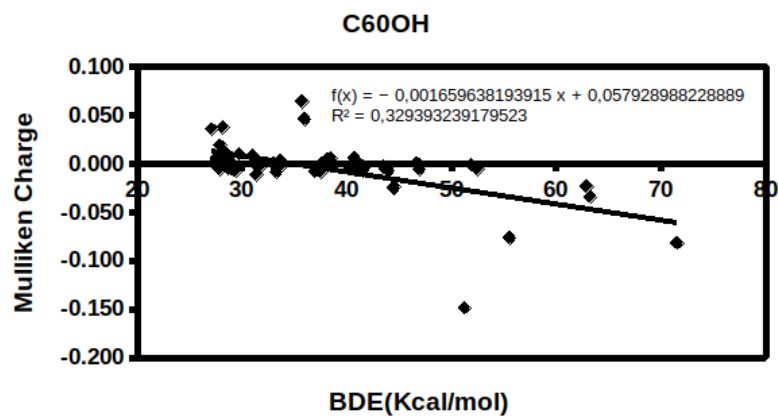
As expected, the numbers in Fig. 7 have near bilateral symmetry with respect to a mirror plane drawn through C1 and C9. Values of $\langle\hat{S}^2\rangle$ vary from 0.00 to about 1.00 (in some cases we see $\langle\hat{S}^2\rangle$ slightly exceeding 1.00). This later value is typical of what is expected for a diradical. Interestingly, the sites with zero spin contamination seem almost, but not quite, to alternate with sites with significant spin contamination. They are also mostly on the front side, rather than the back side, relative to C1. The value of $\langle\hat{S}^2\rangle = 1$ has already been explained by the Lewis dot structure (LDS) shown in Fig. 6. The implications for further reactivity with a third $\bullet\text{OH}$ radical are evident. However, we should remember that the unpaired spins may be widely distributed around the molecule in a way that corresponds to multiple diverse resonance structures in the Lewis representation. The reader is invited to explore which different LDSs may be drawn for each isomer.

Inspection of the “BDE” at $R(\text{C-O}) = 1.4 \text{ \AA}$ relative to a zero of energy at large $R(\text{C-O})$ for symmetry pairs showed that our results are plagued by more numerical problems than is the case for spin contamination. Often these are in cases where spin contamination is high and there might be more than one way to break symmetry. When the BDEs at $R(\text{C-O}) = 1.4 \text{ \AA}$ for symmetry pairs are very different, we also usually find significant differences between the corresponding PECs and $\langle\hat{S}^2\rangle$ curves (shown in the SI). These numerical problems translate into an analysis problem that we have only been able to solve by “cleaning” (i.e., removing from further analysis) symmetry pairs whose BDEs at $R(\text{C-O}) = 1.4 \text{ \AA}$ differ by more than 4 kcal/mol. Specifically, all of the symmetry pairs indicated by an asterisk in Table 1 have been removed from the data. The cleaned results for both $\langle\hat{S}^2\rangle$ and the BDE at $R(\text{C-O}) = 1.4 \text{ \AA}$ are shown in **Fig. 8**. It is seen that $\langle\hat{S}^2\rangle$ is the same in gas phase and in aqueous phase. The gas-phase and aqueous-phase BDE are now linearly related with the BDE being 0.86 kcal/mol higher in the gas phase than in the aqueous phase. This is consistent

(a)



(b)



(c)

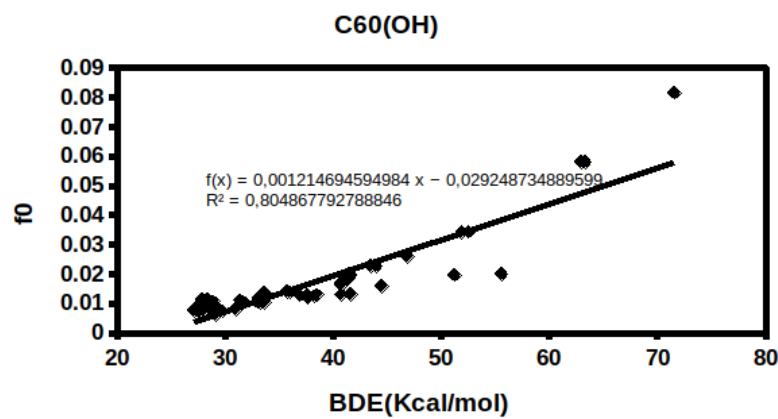


Figure 3: B3LYP(VWN3)/def2SVP/SMD reactivity indices calculated with an implicit solvent model.

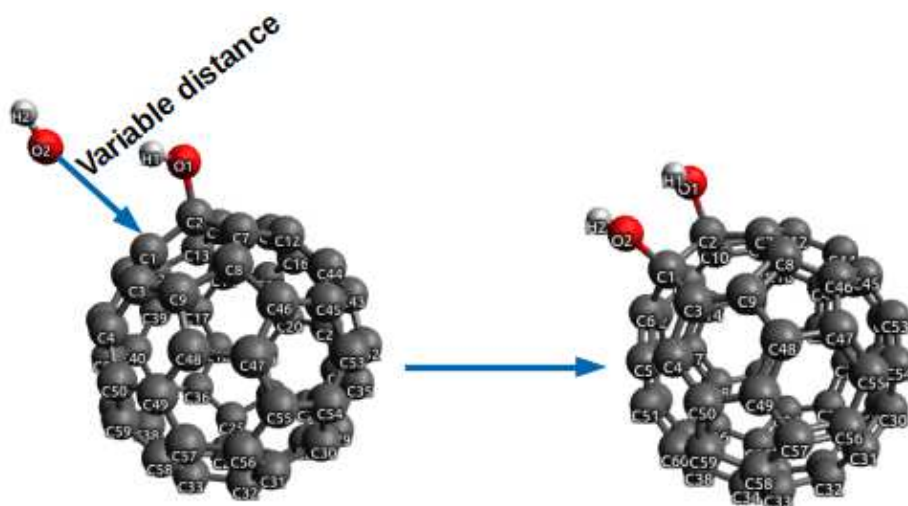


Figure 4: Illustration for isomer 1 of a procedure used for isomers 1, 2, and 3. The vertical docking of $\bullet\text{OH}$ on $\bullet\text{C}_{60}\text{OH}$ was accomplished by beginning from the fullerendiol and using MOLDEN [34] to construct a Z-matrix. Then only the C-O distance was varied for carbon number 1, keeping all other bond and dihedral angles fixed. In particular the structures of $\bullet\text{OH}$ and $\bullet\text{C}_{60}\text{OH}$ were kept fixed.

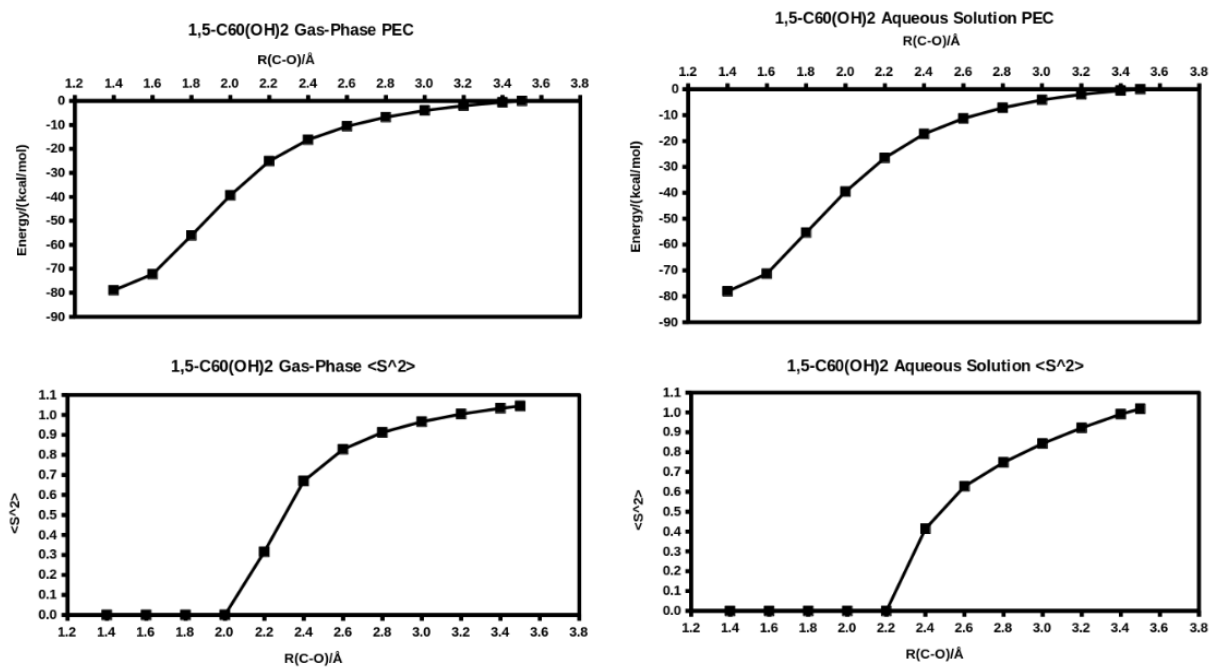


Figure 5: 1,5- $\text{C}_{60}(\text{OH})_2$ (isomer 6) vertical dissociation PECs and spin-contamination for the same geometries in gas phase and in aqueous solution.

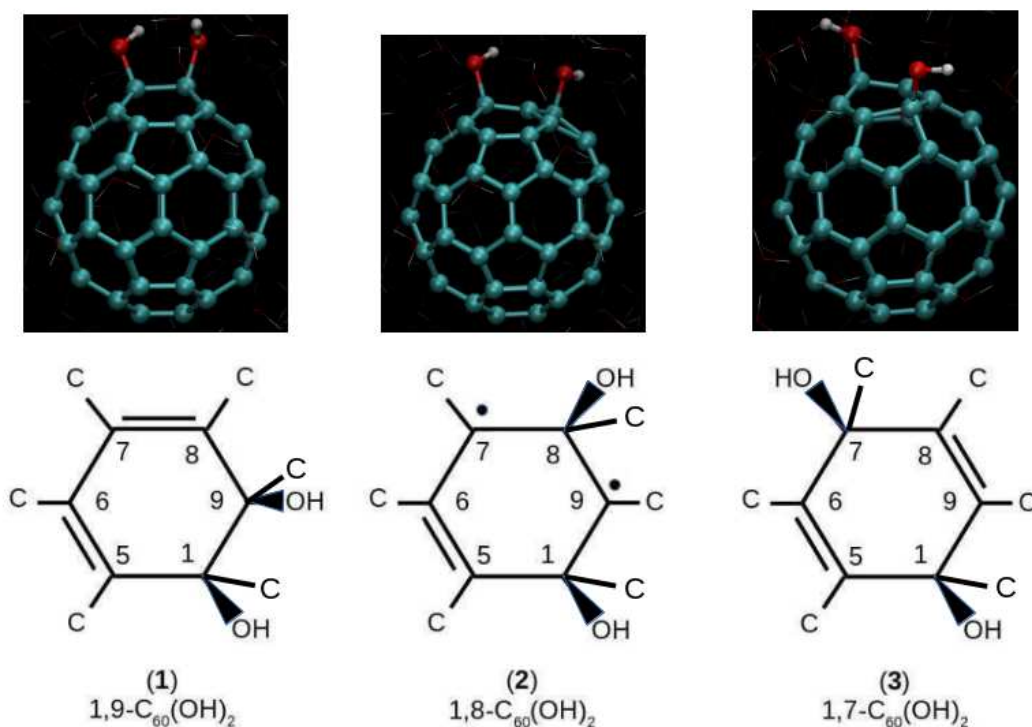


Figure 6: Full (top) and partial (bottom) fullerendiol structures showing the diradical nature of $1,8-C_{60}(OH)_2$. Note that there are several other resonance structures that could be drawn for isomer 2.

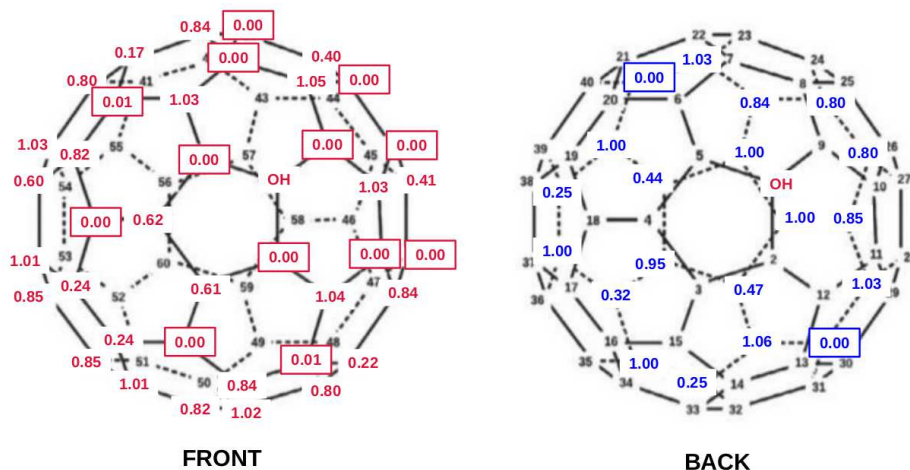


Figure 7: Spin contamination: Averaged over gas-phase and aqueous-phase values, the numbers show the degree of spin-contamination at a C-O distance of 1.4 Å for the *second* OH group. Note that the first OH group is always on carbon 1. It is important to note that the underlying figure is the same as in Fig. 1 because the carbon numbers are obscured by the red and blue numbers showing the value of $\langle \hat{S}^2 \rangle$.

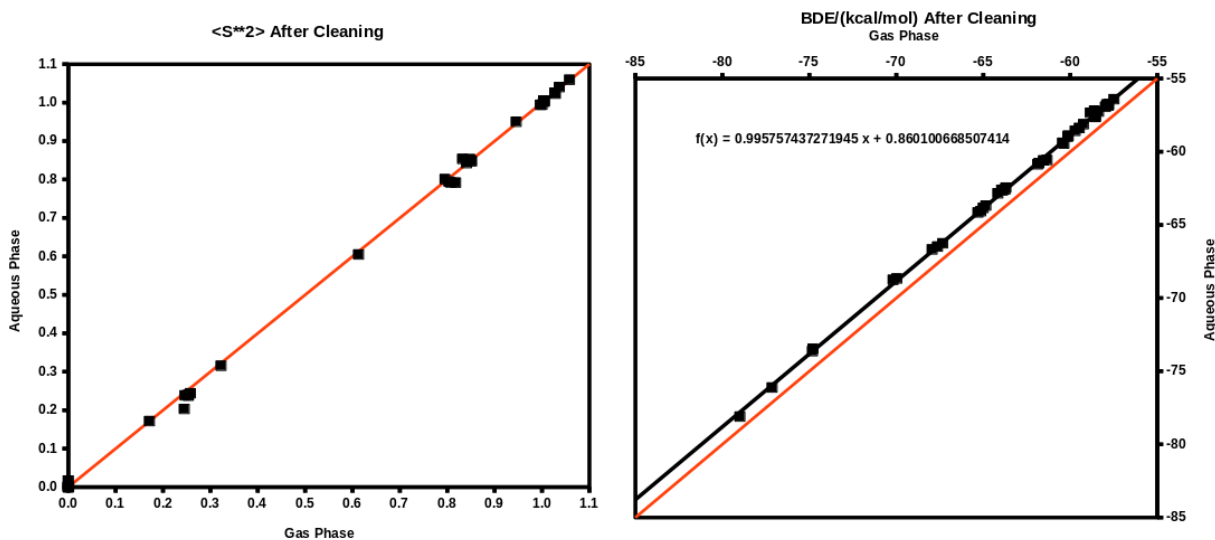


Figure 8: Aqueous-phase versus gas-phase correlation graph of $\langle \hat{S}^2 \rangle$ and BDEs at $R(\text{C-O}) = 1.4 \text{ \AA}$.

with the idea that the products, $\bullet\text{C}_{60}(\text{OH})_2$ and (especially) $\bullet\text{OH}$ are significantly stabilized relative to the reactant $\text{C}_{60}(\text{OH})_2$ in aqueous solution.

Figure 9 provides a closer look at the correlation between the BDE and $\langle \hat{S}^2 \rangle$ in both gas phase and in aqueous solution. For the isomers where $\langle \hat{S}^2 \rangle = 0$, there is a spread of BDEs governed by the chemical reactivity indices discussed above. For $\langle \hat{S}^2 \rangle > 0$, there is a decrease in the BDE as the spin-contimination increases. The functional dependence of the BDE as a function of $\langle \hat{S}^2 \rangle$ seems to be essentially the same in gas and in aqueous solution, even if the BDE in the gas phase is more highly bound by 0.86 kcal/mol.

By now it should be pretty clear that the PECs in gas-phase and in aqueous-phase for a given isomer are very similar. This is illustrated by **Fig. 10** and further illustrated by figures for other isomers given in the SI.

Lastly, in our exploratory work, we wanted to identify at least some of the responsible for the shape of the PECs. We expected the long-distance behavior to go as $1/R^3$ which is typical of a dipole-dipole interaction. Instead we were surprised to see a region with a $1/R^6$ van der Waals interaction-like behavior (**Fig. 11**). There is a simple argument that DFT should be unable to describe the van der Waals $1/R^6$ part of the potential when the electron density of the separated fragments no longer overlap. Our calculations do not contradict this idea as the $1/R^6$ is no longer present at very long distance. However, this is a reminder that a good functional can capture some of the $1/R^6$ behavior at moderately long distance. Indeed one of the challenges when adding van der Waals corrections to DFT is not to overcount any $1/R^6$ behavior that may be already present in the functional.

5 Concluding Discussion

Buckminsterfullerene (C_{60}) is such an excellent radical scavenger that it has been called a “radical sponge” [1]. This makes it interesting as a potential antioxidant for biological applications provided that its solubility can be improved. One way to improve the solubility of C_{60} in water is to add hydroxyl groups which may be done in a variety of ways, including by successive addition of hydroxyl

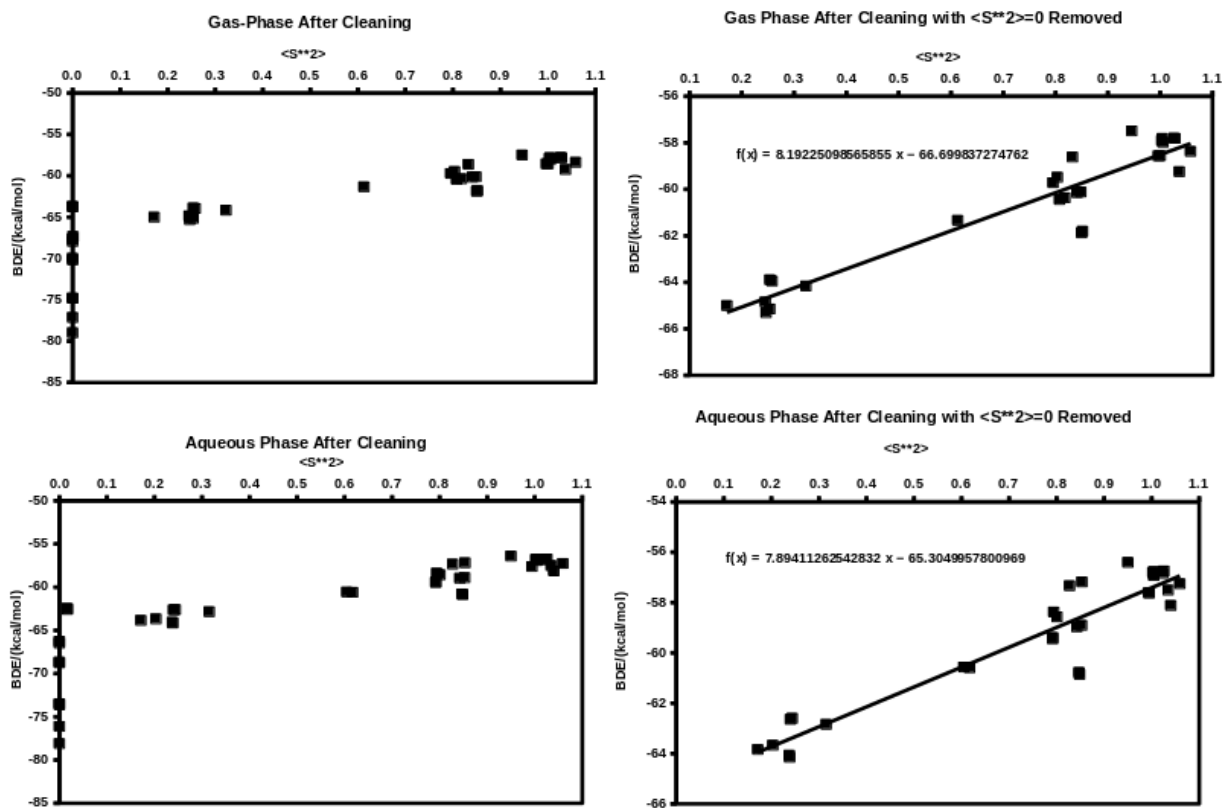


Figure 9: BDEs as a function of $\langle \hat{S}^2 \rangle$ at $R(\text{C-O}) = 1.4 \text{ \AA}$ after data cleaning.

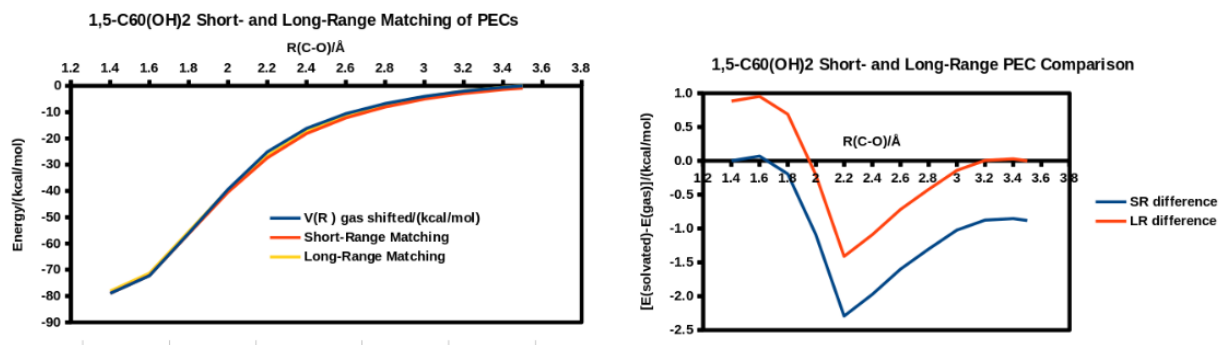


Figure 10: Comparison of the short- and long-range shapes of the solution 1,5-C₆₀(OH)₂ (isomer 6) vertical dissociation PEC with the gas-phase PEC: left, PECs matched at short and long range; right, corresponding solution minus gas phase PEC difference curves.

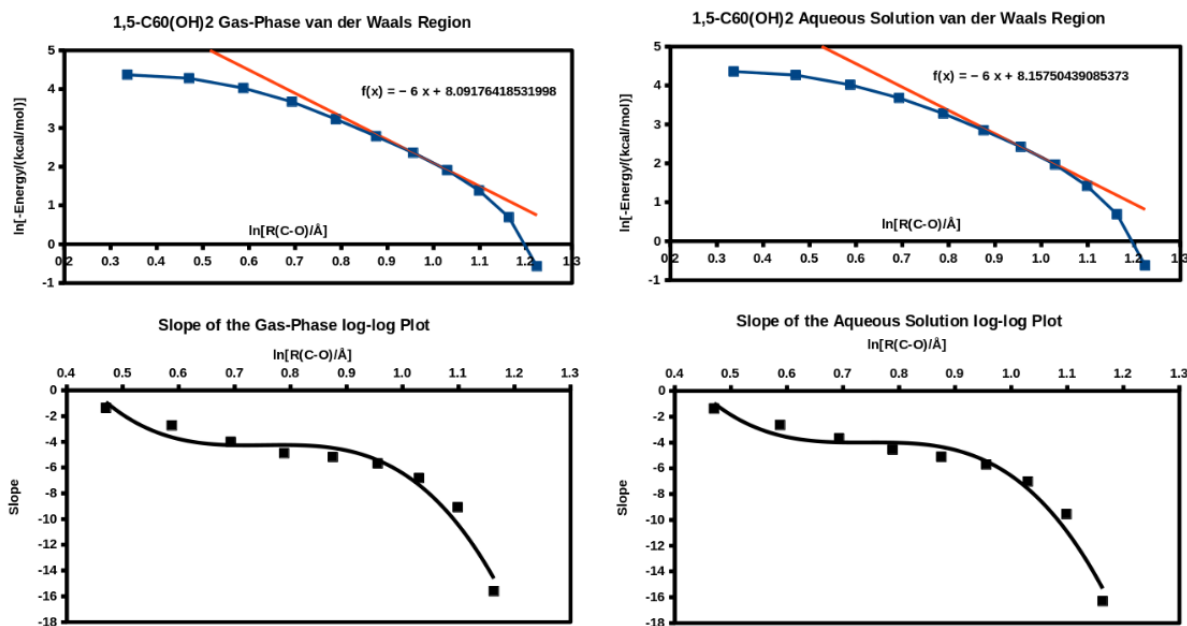


Figure 11: Identification of the van der Waals region of the 1,5- $C_{60}(OH)_2$ (isomer **6**) vertical dissociation PECs. The upper row shows log-log plots of the PEC and tries to “fit” the van der Waals region. The lower row uses a finite difference method to calculate the derivative and then does a least-squares fit to a cubic polynomial.

radicals ($\bullet OH$). The relative stability of different fullerenols ($\bullet C_{60}(OH)_n$ (which is a radical for odd n) has been studied theoretically in previous gas-phase work [16]. Whereas the previous work treated additional fullerenols, the present work is limited to fullerenediols, $C_{60}(OH)_2$. However the present work does extend the previous work in three ways.

Firstly, the SMD implicit solvent model has been used to include the dielectric nature of water, albeit without including the effects of hydrogen bonding. As $C_{60}(OH)_2$ is nearly spherical, we expected that the SMD model would give essentially the same result as the Onsager model which is based upon a spherical cavity. This was shown to be the case. The effect of the implicit solvent model on the dipole moment of the molecule is large and yet calculated reactivity indices show exactly the same qualitative trends as in the gas phase, confirming that $\bullet OH$ is an electrophilic radical [16]. All of these calculations were done using a spin-restricted formalism for $C_{60}(OH)_2$ and a spin-unrestricted formalism for $\bullet C_{60}(OH)$ and for $\bullet OH$.

Secondly, we calculated potential energy curves (PECs) for the dissociation reaction $C_{60}(OH)_2 \rightarrow \bullet C_{60}(OH) + \bullet OH$ in both gas-phase and with the SMD implicit solvent model. This required us to use a spin-unrestricted formalism throughout the reaction path so that the spins could pair up in the same orbitals in $C_{60}(OH)_2$ but separate into different orbitals in the products $\bullet C_{60}(OH) + \bullet OH$. That still left us with a tremendous problem of the dissociation pathway of 59 $C_{60}(OH)_2$ isomers, each of which has multiple conformers. We decided to first carry out a crude vertical dissociation of each isomer which already gave us some very interesting information. In particular, the gas-phase and aqueous-phase PECs turn out to be quantitatively similar.

Thirdly, we noticed that, contrary to our (and we suppose also that of other workers in this field) expectations, it is not always true that $\langle \hat{S}^2 \rangle = 0$ for $C_{60}(OH)_2$. In fact, it is only true for about a quarter of the isomers. We were able to convince ourselves by examining spin densities and

by drawing resonance structures that 1,8-C₆₀(OH)₂ has diradicaloid character and we expect that there must also be di- or even pluriradicaloid character for many of the other fullerenediols. This actually creates a new problem that we did not attempt to address, namely that it is well established that there are several different ways to break symmetry in magnetic clusters and finding the lowest energy broken energy solution is nontrivial. What we did do was to recognize that all but 3 of the fullerenediol isomers come in symmetry pairs and that these almost always give quantitatively similar PECs and graphs of $\langle \hat{S}^2 \rangle$ along the dissociation pathway. This allows us to identify and discard pathways where the symmetry pairs behave too differently (which was the case for only 4 of the isomers). None of the PECs show any convincing evidence of a barrier along their PEC.

While we find it reassuring that many of our conclusions drawn from gas-phase calculations are confirmed in our implicit solvent model, the most important conclusion of the present work is the realization that arbitrary fullerenediols should and do have radicaloid character which should be taken into account by symmetry breaking (as we have done) or by yet more sophisticated linear combination of configuration state functions within some sort of wave function or hybrid wave function/DFT approach.

Acknowledgements

We gratefully acknowledge travel funding for AJE from the U.S.-Africa Initiative [35]. This work was partially funded by NIH R01GM108583 and R35GM151951 to GAC. Computing time for this project was provided by the University of North Texas CASCaM high-performance clusters NSF Grant Numbers CHE1531468 and OAC-2117247, by the NSF Extreme Science and Engineering Discovery Environment, ACCESS project Number TG-CHE160044, and the University of Texas at Dallas' Cyberinfrastructure and Research Services. AP would like to thank Pierre Girard for technical support in the context of the Grenoble *Centre d'Experimentation du Calcul Intensif en Chimie (CECIC)* computers used for the ORCA calculations reported here.

References

- [1] C. N. McEwen, R. G. McKay, and B. S. Larsen, [C₆₀ as a radical sponge](#), *J. Am. Chem. Soc.* **114**, 4412 (1992).
- [2] [The purest carbon 60 oil superantioxidant](https://purec60oliveoil.com/), <https://purec60oliveoil.com/>, Last accessed 5 March 2024.
- [3] Z. Chen, K. Ma, G. Wang, X. Zhao, and A. Tang, [Structures and stabilities of C₆₀\(OH\)₄ and C₆₀\(OH\)₆ fullerenols](#), *J. Mol. Struct. (Theochem)* **498**, 227 (2000).
- [4] J. G. Rodríguez-Zavala and R. A. Guirado-López, [Structure and energetics of polyhydroxylated carbon fullerenes](#), *Phys. Rev. B* **69**, 075411 (2004).
- [5] K. Kokubo, K. Matsubayashi, H. Tategaki, H. Takada, and T. Oshima, [Facile synthesis of highly water-soluble fullerenes more than half-covered by hydroxyl groups](#), *ACS Nano* **2**, 327 (2008).
- [6] E. F. Fileti and R. Rivelino, [The ¹³C NMR properties of low hydroxylated fullerenes with density functional theory](#), *Chem. Phys. Lett.* **467**, 339 (2009).
- [7] J. G. Rodríguez-Zavala, F. J. Tenorio, C. Samaniego, C. I. Méndez-Barrientos, F. G. Peña-Lecona, J. Muñoz-Maciel, and R. Flores-Moreno, [Theoretical study on the sequential hydroxylation of C₈₂ fullerene based on Fukui function](#), *Mol. Phys.* **109**, 1771 (2011).
- [8] H. Ueno, S. Yakamura, R. S. Arastoo, T. Oshima, and K. Kokubo, [Systematic evaluation and mechanistic investigation of antioxidant activity of fullerenols using \$\beta\$ -carotene bleaching assay](#), *J. Nanomater.* **2014**, 802596 (2014).
- [9] K. N. Semenov, N. A. Charykov, V. N. Postnov, V. V. Sharoyko, I. V. Vorotyntsev, M. M. Galaguzda, and I. V. Murin, [Fullerenols: Physiochemical properties and applications](#), *Prog. Solid State Chem.* **44**, 59 (2016).
- [10] S. Afreen, K. Kokubo, K. Muthoosamy, and S. Manickam, [Hydration or hydroxylation: direct synthesis of fulleranol from pristine fullerene \[C₆₀\] via acoustic cavitation in the presence of hydrogen peroxide](#), *RSC Adv.* **7**, 31930 (2017).
- [11] S. Keshri and B. L. Tembe, [Thermodynamics of hydration of fullerols \[C₆₀\(OH\)_n\] and hydrogen bond dynamics in their hydration shells](#), *J. Chem. Phys.* **146**, 074501 (2017).
- [12] M. V. Velarde-Salcedo, M. Gallo, and R. A. Guirado-López, [Low hydroxylated fullerenes: Stability, thermal behavior, and vibrational properties](#), *J. Phys. Chem.* **122**, 13117 (2018).
- [13] Z. Wang, Z. Gao, and Y. Zhao, [Mechanisms of antioxidant activities of fullerenols from first-principles calculation](#), *J. Phys. Chem. A* **122**, 8183 (2018).
- [14] E. S. Kovel, A. A. Sachkova, N. G. Vnukova, G. N. Churilov, E. M. Knyazeva, and N. S. Kudryasheva, [Antioxidant activity and toxicity of fullerenols via bioluminescence signaling: Role of oxygen substituents](#), *Int. J. Mol. Sci.* **20**, 2324 (2019).
- [15] P. Zygouri, K. Spyrou, E. Mitsari, M. Barrio, , R. Macovez, M. Patila, H. Stamatis, I. I. Verginadis, A. P. Velalopoulou, A. M. Evangelou, Z. Sideratou, D. Gournis, and P. Rudolf, [A facile approach to hydrophilic oxidized fullerenes and their derivatives as cytotoxic agents and supports for nanobiocatalytic systems](#), *Scientific Reports* **10**, 8244 (2020).

- [16] A. Ponra, A. J. Etindele, O. Motapon, and M. E. Casida, [Binding energies for successive addition reaction of \$\bullet\text{OH}\$ with \$\text{C}_{60}\$: A laboratory for testing frontier molecular orbital theory](#), *Adv. Quant. Chem.* **8**, 2023 (2023).
- [17] A. Moreno-Ceballos, M. E. Castro, N. A. Caballero, L. Mammimo, and F. J. Melendez, [Implicit and explicit solvent effects on the global reactivity and the density topological parameters of the preferred conformers of caespitate](#), *Computation* **12**, 5 (2024).
- [18] P. P. Fehér and A. Stirling, [Assessment of reactivities with explicit and implicit solvent models: QM/MM and gas-phase evaluation of three different Ag-catalysed furan ring formation routes](#), *New J. Chem.* **43**, 15706 (2019).
- [19] A. Ponra, A. J. Etindele, O. Motapon, and M. E. Casida, [Practical treatment of singlet oxygen with density-functional theory and the multiplet-sum method](#), *Theo. Chem. Acc.* **140**, 154 (2021).
- [20] A. Ponra, C. Bakasa, A. J. Etindele, and M. E. Casida, [Diagrammatic multiplet-sum method \(MSM\) density-functional theory \(DFT\): Investigation of the transferability of integrals in "simple" DFT-based approaches to multi-determinantal problems](#), *J. Chem. Phys.* **159**, 244306 (2023).
- [21] A. V. Marenich, C. J. Cramer, and D. G. Truhlar, [Universal solvation model based on solute electron density and on a continuum model of the solvent defined by the bulk dielectric constant and atomic surface tensions](#), *J. Phys. Chem. B* **113**, 6378 (2009).
- [22] L. Onsager, [Electric moments of molecules in liquids](#), *J. Am. Chem. Soc.* **58**, 1486 (1936).
- [23] M. ea Frisch, [Gaussian 16 revision a. 03](#), 2016.
- [24] C. J. F. Böttcher, *Theory of Electric Polarization, Vol. I, Dielectrics in Static Fields*, Elsevier Scientific Publishing Company, New York, 1973.
- [25] E. M. Purcell, *Electricity and Magnetism*, volume 2 of *Berkeley Physics Series*, McGraw-Hill, New York, 1963.
- [26] D. Huffman, [Solid \$\text{C}_{60}\$](#) , *Physics Today* **44**, 22 (1991).
- [27] W. M. Powell, F. Cozzi, G. P. Moss, C. Thilgen, R. J. Hwu, and A. Yerin, [Nomenclature for the \$\text{C}_{60} - I_h\$ and \$\text{C}_{70} - D_{5h\(6\)}\$ fullerenes \(IUPAC recommendations \(2002\)\)](#), *Pure Appl. Chem.* **74**, 629 (2002).
- [28] F. Neese, [Software update: The ORCA program system, version 4.0](#), *Wiley Interdisciplinary Reviews: Computational Molecular Science* **8**, e1327 (2018).
- [29] A. D. Becke, [Density-functional thermochemistry. III. The role of exact exchange](#), *J. Chem. Phys.* **98**, 5648 (1993).
- [30] C. Lee, W. Yang, and R. G. Parr, [Development of the colle-salvetti correlation-energy formula into a functional of the electron density](#), *Phys. Rev. B* **37**, 785 (1988).
- [31] F. Weigend and R. Ahlrichs, [Balanced basis sets of split valence, triple zeta valence and quadruple zeta valence quality for H to Rn: Design and assessment of accuracy](#), *Phys. Chem. Chem. Phys.* **7**, 3297 (2005).

- [32] D. Magero, A. M. H. M. Dargouth, and M. Casida, [Test of the orbital-based LI3 index as a predictor of the height of the \$^3\text{MLCT} \rightarrow ^3\text{MC}\$ transition-state barrier for gas-phase \$\[\text{Ru}\(\text{N}\wedge\text{N}\)_3\]^{2+}\$](#) , *J. Photochem. Photobio. A: Chem.* **451**, 115502 (2024).
- [33] A. M. H. M. Dargouth, D. Magero, and M. E. Casida, [Test of the orbital-based LI3 index as a predictor of the height of the \$^3\text{MLCT} \rightarrow ^3\text{MC}\$ transition-state barrier for \$\[\text{Ru}\(\text{N}\wedge\text{N}\)_3\]^{2+}\$ polypyridine complexes in \$\text{CH}_3\text{CN}\$](#) , *J. Phys. Chem. A* **XXX**, yyyyyy (2024?).
- [34] B. Schaftenaar, [MOLDEN: A pre- and post processing program of molecular electronic structure](#), <https://www3.cmbi.umcn.nl/molden/>, Last accessed 22 May 2021.
- [35] [U.S.-Africa Initiative](#), <https://usafricainitiative.org>, Last accessed 20 February 2020.